Journal of Thermal Analysis and Calorimetry

Kinetic of Pyrite thermal degradation under oxidative environment

--Manuscript Draft--

Manuscript Number:	JTAC-D-19-00517
Full Title:	Kinetic of Pyrite thermal degradation under oxidative environment
Article Type:	Research Paper
Abstract:	Pyrite is the most common mineral in polymetallic sulphides ores. In order to apply the combustion group theory to the pyrometallurgical processes that occur in the reaction shaft it is necessary to know the kinetic processes that happen in pyrite. In this study a thermogravimetric analysis was carried out under oxidative atmospheric conditions with 100% O2 and a heating ramp of 5, 10, 15 and 20 ºC min-1. The material used was pyrite with a grain size of 63-125 µm. From the thermogravimetric data we got the kinetic parameters of the oxidative reactions of pyrite. The different kinetic methods used in this study have been E1641-16 ASTM, Ozawa-Flynn-Wall, Kissinger-Akahira-Sunose and Friedman. These methods were used for obtaining the kinetic parameters through Regression analysis, Sum of squares, mean residuals between experimental and calculated values and Student coefficient (95%) and to determine which kinetic method is the most suitable to describe the kinetics of pyrite oxidation.

Kinetic of Pyrite thermal degradation under oxidative environment

Vázquez, M. [1], Moreno-Ventas, I.[1], Raposo, I.[1], Palma, A.[2], Díaz, M.J.[2]

[1]Facultad de Ciencias Experimentales, University of Huelva, Huelva, 21007, Spain. Centro de Investigación en Química Sostenible (CIQSO), University of Huelva, Huelva, 21007, Spain
[2]Escuela Técnica Superior de Ingeniería, University of Huelva, Huelva, 21007, Spain. Centre for Research in Product Technology and Chemical Processes (Pro2TecS), University of Huelva, Huelva, 21007, Spain

Moreno-Ventas, I. (https://orcid.org/0000-0002-7927-5212), Palma, A. (https://orcid.org/0000-0003-0420-1785), Díaz, M,J. (https://orcid.org/0000-0002-5059-4340)

Abstract:

Pyrite is the most common mineral in polymetallic sulphides ores. In order to apply the combustion group theory to the pyrometallurgical processes that occur in the reaction shaft it is necessary to know the kinetic processes that happen in pyrite. In this study a thermogravimetric analysis was carried out under oxidative atmospheric conditions with 100% O_2 and a heating ramp of 5, 10, 15 and 20 ºC min^{-1}. The material used was pyrite with a grain size of 63-125 µm. From the thermogravimetric data we got the kinetic parameters of the oxidative reactions of pyrite. The different kinetic methods used in this study have been E1641-16 ASTM, Ozawa-Flynn-Wall, Kissinger-Akahira-Sunose and Friedman.

These methods were used for obtaining the kinetic parameters through Regression analysis, Sum of squares, mean residuals between experimental and calculated values and Student coefficient (95%) and to determine which kinetic method is the most suitable to describe the kinetics of pyrite oxidation.

Keywords: Pyrite, Thermogravimetry, Sulphide, Kinetic, Ozawa-Flynn-Wall, Kissinger-Akahira-sunose, Friedman, ASTM-E1641.

1. Introduction

Pyrite (FeS_2) is the most common mineral in sulphide ores. It is composed of 53.48% sulphur and 46.52% iron [1] and it has cubic structure with unit-cell edge around 5.42Å. Usually appears in association with other minerals such as chalcopyrite ($CuFeS_2$), galena (PbS), tetraedrite ($Cu_6[Cu_4(Fe,Zn)_2]Sb_4S_{13}$), chalcocite ($Cu_2S$) and sphalerite (ZnS) [2].

To use polymetallic sulphides in extractive copper pyrometallurgical processes it is necessary to enrich sulphide ores in copper through grinding and flotation techniques in order to have from deposits with a copper concentration of 0.5-2 Wt. % Cu to a material called "concentrates" (Fig.1) with a copper concentration of 20-30 Wt. % Cu [3, 4].

Fig. 1: BSE (Back-scattered Electron) image of a concentrate obtained through an electronic microprobe model JEOL, model JXA-8200 Super probe. Working conditions used were an acceleration voltage of 15 kV and a current of 20 ~~nA~~ Å of beam intensity with an electron beam diameter between 1 and 5 µm. Py: Pyrite (FeS2), Dg: Digenite (Cu9S5), Mb: Molybdenite (MoS2).

The concentrates are mixed forming blends, to get a regular composition in order to carry out the pyrometallurgy processes.

Oxidative melting of the blend is made through two stages (Flash smelting and conversion processes) in order to minimize copper losses. [3].

In the first stage, two immiscible liquids are produced through flash smelting: matte and slag [5]. Matte is a sulphidic melt composed of FeS and Cu_2S (usually the matte grade is around 62 wt.% Cu). Slag melts are composed mainly of fayalite (Fe_2SiO_4) and magnetite (Fe_3O_4) in a proportion that depends on oxygen partial pressure (usually 10^{-7} atm for flash smelting).

The liquid immiscibility region between slag and matte was shown in the experimental work of Yazawa and Kameda [6] over the ternary system of SiO_2-FeO-FeS (Fig. 2).

Fig. 2: Isothermal phase diagram (FeO-FeS-SiO_2) from Yazawa and Kameda [6]. Point A and B are in equilibrium and marks, respectively, the composition of an oxide rich melt (slag) and the composition of a sulphide rich melt (matte). Both compositions, A and B correspond to a system in the limit of silica solubility. To the right of line A-B the immiscible melts coexist with solid silica.

As it is ~~showed~~ in the FeO-FeS-SiO_2 phase diagram, the blends are brought into the immiscibility region by adding SiO_2 (arrow in bold in Figure 2) as a flux component for melting. The ~~main~~ to take the system inside the liquid immiscibility region is the extraction of part of the iron to the slag and the copper to the matte.

After the first stage, the conversion process ~~transform~~ the matte melts in blister copper through two oxygen-blowing stages. In the first stage (slag blowing) the oxygen reacts with FeS to produce iron and sulphur dioxide. At the same time, iron reacts with the silica flux to make fayalite (Fe_2SiO_4). This blowing stage produce white metal melt (Cu_2S) (Eq.1):

$$Cu_2S + 2FeS + SiO_2 + 3O_2 \rightarrow Cu_2S + Fe_2SiO_4 + 2SO_2 \quad \text{(Eq. 1)}$$

The white metal produced in slag blowing is used to get copper blister through the second stage of oxidation named Copper blowing [7] (Fig. 3).

Fig. 3: Equilibrium phase diagram from Sharma and Chang [7]. The dotted line marks the different compositions (Points a, b, c and d) of the conversions process at 1200ºC in copper blowing.

The equilibrium phase diagram (Fig. 3) shows the copper blowing stage at 1200 °C. Beginning with the white metal (Point a) the system goes into a new liquid immiscible region to give molten blister copper plus molten white metal. As the oxidative process goes on the proportion of blister copper increase from point b to point c generating an SO_2 gas phase.

Schematically, the conversion process follows the next reaction (Eq. 2):

$$(Cu, Fe, S)(molten\ matte) + O_2(in\ ~~oxigen~~\ enriched\ air) + SiO_2(solid\ flux) \rightarrow Cu^0(l) + 2FeO \cdot SiO_2(in\ molten\ slag) + Fe_3O_4(in\ molten\ slag) \quad \text{(Eq. 2)}$$

Oxidative melting of blends is controlled by the ignition temperature and kinetic of the combustion of sulphides that occurs in the reaction shaft in flash smelting processes (first oxidation stage of blends). Ignition of blends is an exothermic process that starts for the most reactive sulphide grains and spread to the rest of grains through radiative heat flow. The application of the group theory of combustion to the flash smelting process ~~needs of~~ data about the kinetics of sulphides species.

Most of the studies carried out about the TGA literature on sulphides focus on the analysis of the reaction mechanisms of oxidation processes, the different thermogravimetric behavior of minerals against variations in mineral grain sizes, intrinsic water content or differences in the composition of the ~~air~~ [8-13].

In this study it is analyzed the reaction kinetics of the pyrite oxidation process, by studying different kinetics methods to determine which kinetic method is the most suitable for use with pyrite, from thermogravimetry studies performed on pyrite minerals. The kinetics methods used are E1641-16 [14], Ozawa/Flynn/Wall [15-17], Kissinger-Akahira-Sunose (KAS) [18, 19] and Friedman [20].

2. Materials and Methods

2.1. Raw materials

The composition of the pyrite is usually pure although in some occasions there may be substitutions of metallic elements such as Ni, Co or more rarely Cu replacing the Fe.

The pyrites are quite chemically stable, we checked it by studying 40 different pyrite compositions obtained through the RRUFF database [1]. This similarity of compositions gives us that the thermogravimetry study is significant and it has a wide validity because there are no variations in the composition.

The average composition of the pyrites, according to the Rruff database is 46.76% Fe and 53.24% S.

The pyrite was crushed and ~~screened~~ into the fraction 63-125 µm for used in the study.

The pyrite sample used for the study was analyzed by x-ray diffraction model BRUKER D8 Advance, in Bragg-Brentano geometry, using copper Kα radiation (Kα = 1,5406 Å) excited by a current of 30 mA of intensity and 40 kV of voltage. The working conditions were ~~a~~ scan interval of 3 to 65º of 2 Θ, an increase of angle step of 0.2º of 2 Θ, and an exposure time per step of 0.6s.

The treatment and evaluation of diffractometry data is done using the DIFFRACplus software and XPowder.12 software used with the database AMSCD (American Mineralogist Crystal Structure Database).

The diffractogram obtained shows that the sample used during the study was of pyrite composition. (Fig. 4).

Fig. 4: Pyrite diffractogram pointing to the D-Spacing in amperes.

2.2. TGA experiments

A thermo-gravimetric analyzer (TGA) and differential scanning calorimetry (DSC) (Mettler Toledo TGA/DSC1 STARe System) has been used to study pyrite thermo-chemical oxidation behavior. Both experiments were performed by heating a 70-130 mg sample under a temperature range of 25-900°C and four heating rates of 5, 10, 15 and 20°C min^{-1} and 20 cm^3 min^{-1} oxygen flow has been also used. Pyrite oxidation kinetic data such as Arrhenius activation energy (E_a) and pre-exponential constant (A) from TGA data have been calculated by using four proven free isoconversional methods such as: E1641–16 [14], Ozawa/Flynn/Wall [15-17], Kissinger-Akahira-Sunose (KAS) [18, 19] and Friedman [20] models. In this form, the reactions processes could be found without the assumption of any kinetic model. NETZSCH Kinetics Neo® software has been used to analyze thermo-chemical processes data. Among above mentioned studied methods, the better statistical data obtained have been exposed.

3. Results and Discussion

3.1. Thermogravimetric analysis of the thermochemical process.

The TGA and DTG (first derivative TGA curve) for pyrite (mean of the two replicates per heating rate) over the range of temperature from 25ºC to 850ºC under four heating rates (5, 10, 15 and 20 ºC min^{-1}) and oxygen atmosphere are shown in Figures 5 and 6 respectively. The Fig 5 and 6 show that different results, for each studied heating rate, are obtained. Main differences in the obtained curve at 5ºC/min have been observed. In general, TGA curves show that the oxidation reactions for pyrite in a range from 440-500ºC and from 500-850ºC approximately have been observed. Specifically, an initial pyrite degradation at 440ºC (Fig. 6), with a loss of mass (approximately 30% of the initial mass) have been observed in Fig. 5. According to Zivkovic et al. [21] the first degradation could be due to a pyrite dissociation following Eq. 3. In this sense, it is worth mentioning that in the study carried out by Zivkovic et al., [21] the first loss of mass occurred at 370ºC, Earnest [22] described the degradation at 400ºC, Pérez et al., [13] among 485 to 625ºC, Dunn et al., [23] among 425-435ºC and Dunn [24], among 330 to 630ºC. The obtained sulphur, under an oxidative atmosphere, had been oxidized to SO_2 (Eq. 4) and the oxidation of FeS_2 to magnetite (Fe_3O_4, Eq.5) could also have taken place at that temperature.

Fig. 5: Thermal gravimetric analysis of pyrite with 100% O_2.

Fig. 6: Differential thermal gravimetric analysis of pyrite with 100% O_2.

$$2FeS_2(s) \rightarrow 2FeS(s) + S_2(g) \quad \text{(Eq. 3)}$$

$$S_2(g) + 2O_2(g) \rightarrow 2\,SO_2(g) \quad \text{(Eq. 4)}$$

$$FeS_2(s) + \frac{8}{3}O_2(g) \rightarrow \frac{1}{3}Fe_3O_4(s) + 2O_2(g) \quad \text{(Eq. 5)}$$

After the first degradation phase, under an increase in temperature (≈480ºC), occurred a sulphation (Eq. 6 and magnetite was oxidized to hematite (Eq. 7), which leads to a slight increase (0.3% of the initial mass) in mass (Fig 6),

$$FeS(s) + 2O_2(g) \rightarrow FeSO_4(s) \quad \text{(Eq. 6)}$$

$$4Fe_3O_4(s) + O_2(g) \rightarrow 6Fe_2O_3(s) \quad \text{(Eq. 7)}$$

Under high temperatures (≥650ºC) the formed iron (II) sulphate was degraded (approximately 3.5% of the initial mass) into hematite (iron (III) oxide, Eq. 8)

$$2FeSO_4(s) \rightarrow Fe_2O_3(s) + SO_2(g) + SO_3(g) \quad \text{(Eq. 8)}$$

3.2. Analysis of pyrite oxidation kinetics

The kinetic parameters were calculated by using the above mentioned model-free methods. As expected, not all studied models are in agreement to an adequate fit for the oxidative degradation of pyrite. Thus, in Table 1 the main statistical values (regression analysis, sum of deviation squares, mean residuals between experimental and calculated values and Student coefficient) calculated from the models are shown.

From Table 1, among the studied methods Kissinger's method seems to be the most adequate to describe the oxidative thermal behavior of pyrite.

The KAS method [19] (Eq. 9) is an extension to the 0.1-0.9 interval of the initial Kissinger model [18]. In this sense, KAS's kinetic method is an isoconversional method where the activation energy is a function of the conversion degree of a chemical reaction and can be applied without any assumption concerning the kinetic model f(α).

$$\ln\left(\frac{\beta_i}{T_{jk}^2}\right) = \ln\left(\frac{A_{0\alpha}R}{E_{a\alpha}}\right) - \frac{E_{a\alpha}}{RT_{jk}} - \ln g(\alpha_k) \quad \text{Eq. 9}$$

where $E_{a\alpha}$ and $A_{0\alpha}$ are the apparent activation energy and the pre-exponential factor at a given conversion degree α_k, and the temperatures T_{jk} are those which the conversion α_k is reached at a heating rate β_j. for a

series of experiments at different heating rates (β). In this form, T_{jk} is the temperature peak of the DTG curve and a series of different heating rate measurements are ($\beta_{i,j}$) required in this model (Fig. 7).

Fig. 7: Kissinger-Akahira-Sunose plot of pyrite.

The apparent activation energy and Arrhenius pre-exponential factor (under different conversion grade) could be obtained from the slope and the intercept, respectively, of the linear plot of $\ln\left(\beta_i / T_{jk}^2\right)$ *vs.* $1/T_{jk}$.

According to Eq. 9 several conversion (α) values (0.1 to 0.9) for all curves (different heating rates) have been evaluated. The KAS equation (slope and R^2) shows a high relationship between ~~of~~ ln (β_i/T_{jk}^2) and $1000/T_{\alpha i}$ (Fig. 7). Therefore, method is considered suitable for obtaining the activation energy for thermochemical oxidation of pyrite. After that, apparent activation energy (E_a) values could be assessed from the slopes of these equations for each α. As shown in Figure 7, the obtained slopes, and therefore, the calculated values for apparent Ea, regardless of the rate of heating, appear to be similar. To determine the kinetic parameters, we chose the value of α from range 0.1 to 0.9 on the curve obtained at 15ºC min^{-1} (medium value) heating rate. In Figure 8, the calculated E_a values results show that the activation energy was not similar for all conversion indicates the existence of a complex mechanism that occurs in the solid state.

Fig. 8: Apparent activation energy (Ea) values for pyrite thermal oxidative degradation calculated from the KAS equation for each conversion grade (α) value.

In Figure 9 an evolution of the pre-exponential factor (A) is shown. t is important to note that, according to Vyazovkin [25], model-free kinetic models have the inconvenient to treating the experimental value of A as a dependent parameter. In this sense, similar behavior to that described for Ea, can be observed for this parameter.

Fig. 9: ~~Fig. 12:~~ Pre-exponential factor (A) values calculated from the KAS equation for each conversion grade (α) value.

The obtained E_a and A values were highly dependent on the extent of conversion which could indicate that the process must be described as a multi-step reaction. The calculated E_a and A values at the different

conversion rates show higher values under low conversion degree (200-450 kJ mol^{-1}). The initial increase in activation energy conversion may be attributed to ignition and pyrite oxidation (Eq. 3-5). After that, a progressive decline to values close to 80 kJ mol^{-1} at α=0.8 is found. The lower kinetic values of E_a and A values obtained in under high conversion values, compared to those obtained in the initial reaction zone, may be due to the fact that magnetite ~~which~~ had lower decomposition rate than cellulose and hematite. There may also have been a catalytic effect from inorganic elements on that degradation.

4. Conclusions

Thermal degradation kinetic for oxidation process of pyrite have been studied in TGA by using E1641–16, Ozawa/Flynn/Wall, Kissinger-Akahira-Sunose and Friedman models.

The most suitable model, among those studied, seems to be the one proposed by Kissinger.

The oxidation process of pyrite can be described as a multi-step reaction because values of Ea and A were highly dependent on the degree of conversion.

The calculated Ea values ranged among 450 kJ mol^{-1} at α= 0.3 and 80 kJ mol^{-1} at α= 0.8.

5. References

[1] RRUFF™ Project database http://rruff.info/pyrite/display=default/ (accessed 13 March 2019)

[2] Zussman J, Howie RA, Deer WA. An introduction to the rock forming minerals. An Introduction to the Rock-Forming Minerals, 2nd edition. London (Longman Scientific and Technical). 1992. https://doi.org/10.1180/minmag.1992.056.385.20.

[3] Schlesinger ME, King MJ, Sole KC, Davenport WG. Extractive Metallurgy of Copper. Elsevier Science. London. 2011.

[4] Sancho JP, Verdeja LF, Ballester A. Metalurgia Extractiva. Volumen II: Procesos de obtención, Edited by Sintesis, Madrid, Spain, ISBN 84-7738-803-2. 2000.

[5] Davenport WG, Jones DM, King MJ, Partelpoeg EH. Flash Smelting: Analysis, Control and Optimization. 2th Ed. T The Minerals, Metals and Materials Society (TMS). Pittsburgh, PA. 2003.

[6] Yazawa A, Kameda A, Copper Smelting. I. Partial liquidus diagram for FeSFeO-SiO2 system. Tech Rep Tohoku Univ. 1953;16: 40-58.

[7] Sharma RC, Chang YA. A thermodynamic analysis of the copper sulfur system. Metall Transac B. 1980; 11B: 575-583.

[8] Dunn JG, Jayaweera SAA. Applications of thermoanalytical methods to studies of flash smelting reactions. Thermochim Acta. 1985. https://doi.org/10.1016/0040-6031(85)85543-X

[9] Dunn JG, De GC, O'Connor BH. The effect of experimental variables on the mechanism of the oxidation of pyrite: Part 1. Oxidation of particles less than 45 μm in size. Thermochim Acta. 1989; 145: 115-130.

[10] Reimers GW, Hjelmstad KE. Analysis of the oxidation of chalcopyrite, chalcocite, galena, pyrrhotite, marcasite and arsenopyrite. Dept. of the Interior, Bureau of Mines. Report of investigations (United States. Bureau of Mines): 1987; 9118. Pittsburgh, Pa. U.S.

[11] Jorgensen FRA, Moyle FJ, Wadsley MW. Structural changes associated with the ignition of pyrite and chalcopyrite during flash smelting. In: Process Mineralogy IX, International symposium of Applied Mineralogy MAC-ICAM-CAN. 1989; 14-17 May. Montreal. CA. 323-341,

[12] Perez-Tello M, Sohn HY, Löttiger J. Determination of the oxidation characteristics of solid copper matte particles by differential scanning calorimetry and thermogravimetric analysis. Mining Metall Explorat. 1999. https://doi.org/10.1007/BF03402800.

[13] Pérez-Fontes SE, Pérez-Tello M, Prieto-López LO, Brown F, Castillón-Barraza F. Thermoanalytical study on the oxidation of sulfide minerals at high temperatures. Min Metal Process. 2007. https://doi.org/10.1007/bf03403377.

[14] ASTM Test Method E1641. Standard Test Method for Decomposition Kinetics by Thermogravimetry, ASTM Book of Standards 14.02, American Society for Testing and Materials, pp. 1042-1046. 1994.

[15] Ozawa T. A new method of analyzing thermogravimetric data, Bull Chem Soc Jap. 1965. https://doi.org/10.1246/bcsj.38.1881.

[16] Ozawa T (1965) Kinetic analysis of derivative curves in thermal analysis. J Thermal Anal Calorim 2 (3): 301-324. https://doi.org/10.1007/BF01911411.

[17] Flynn J, Wall L. A quick, direct method for the determination of activation 0energy from thermogravimetric data. Journal of Polymer Science Part B: Polym Let. 1966; 4 (5): 323-328.

[18] Kissinger HE. Variation of peak temperature with heating rate in differential thermal analysis. J Res Nat Bur Stand. 1956. https://doi.org/10.6028/jres.057.026.

[19] Akahira T, Sunose T. Method of determining activation deterioration constant of electrical insulating materials. Res Report Chiba Inst Technol (Sci Technol). 1971; 16: 22-31.

[20] Friedman HL. Kinetics of thermal degradation of char-forming plastics from thermogravimetry. Application to a phenolic plastic. J Polym Sci Part C. 1964; 6: 183-195.

[21] Živković ŽD, Mitevska N, Savović V. Kinetics and mechanism of the pyrite-pyrite concentrate oxidation process. Thermochim Acta. 1996. https://doi.org/10.1016/0040-6031(96)02883-3.

[22] Earnest CM. Descriptive oxidative profiles for pyrite in the low temperature ash component of coals by differential thermal analysis. Thermochim Acta. 1984; 75(1-2): 219-232.

[23] Dunn JG, De GC, O'Connor BH. The effect of experimental variables on the mechanism of the oxidation of pyrite: Part 2. Oxidation of particles of size 90–125 μm. Thermochim Acta. 1989; 155: 135-149.

[24] Dunn JG. The oxidation of sulphide minerals. Thermochim Acta . 1997; 300 (1-2): 127-139.

[25] Vyazovkin S. Model-free kinetics. Staying free of multiplying entities without necessity. J Therm Anal Calorim. 2006. https://doi.org/10.1007/s10973-005-7044-6.

Figure 1

Click here to access/download;Figure;Fig 1 (BSE image).png

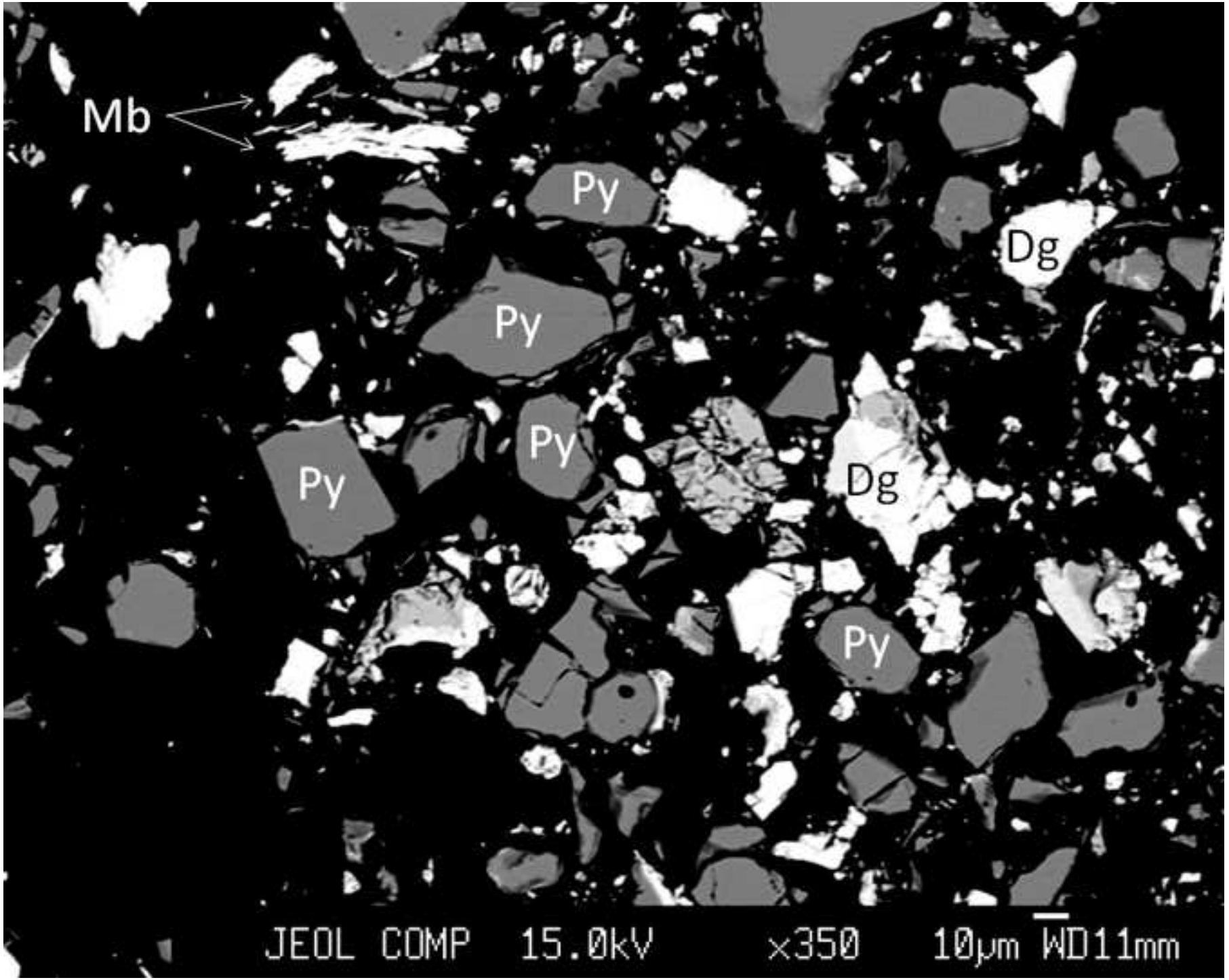

Figure 2

Click here to access/download;Figure;Fig 2 (Yazawa & kameda).png

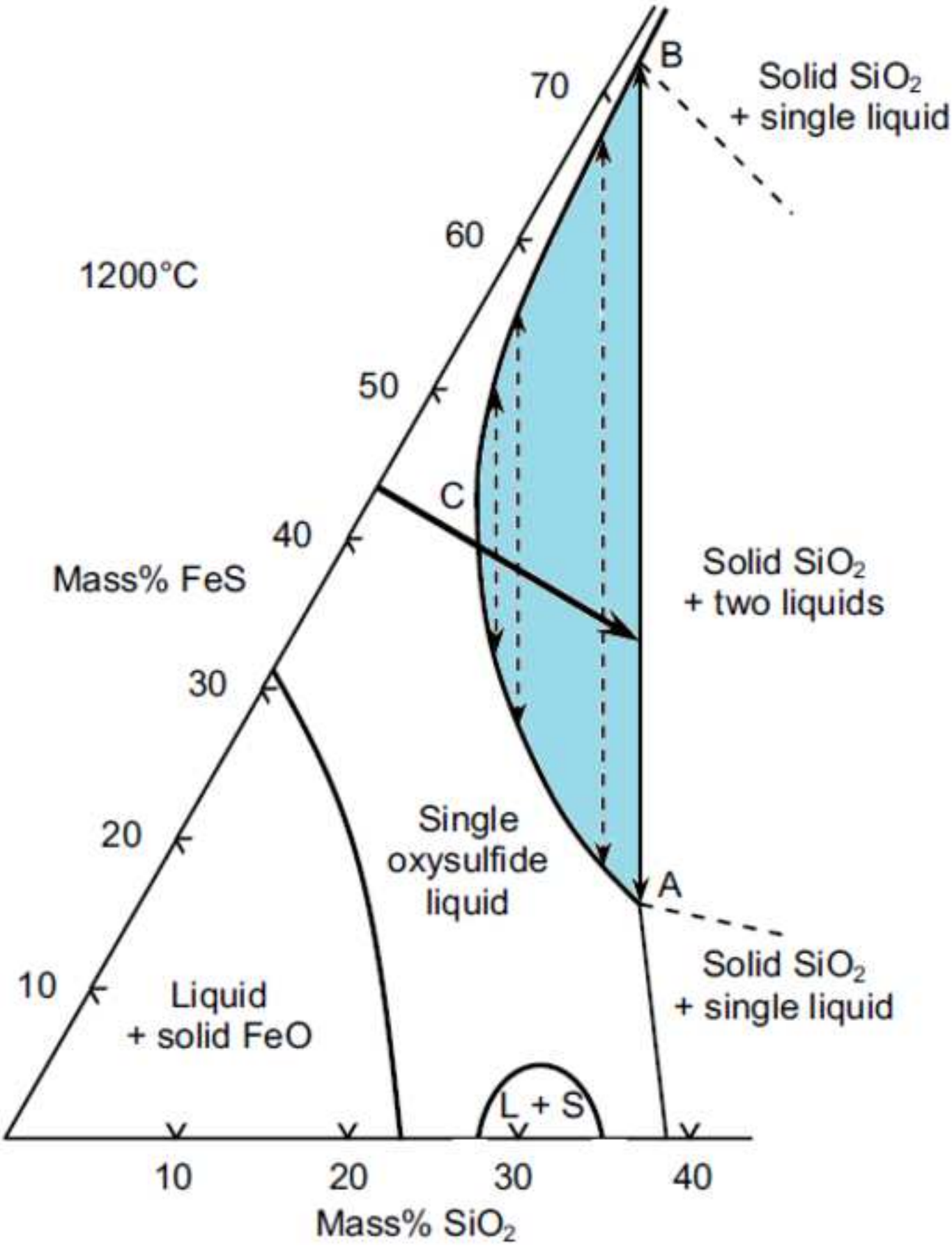

Figure 3

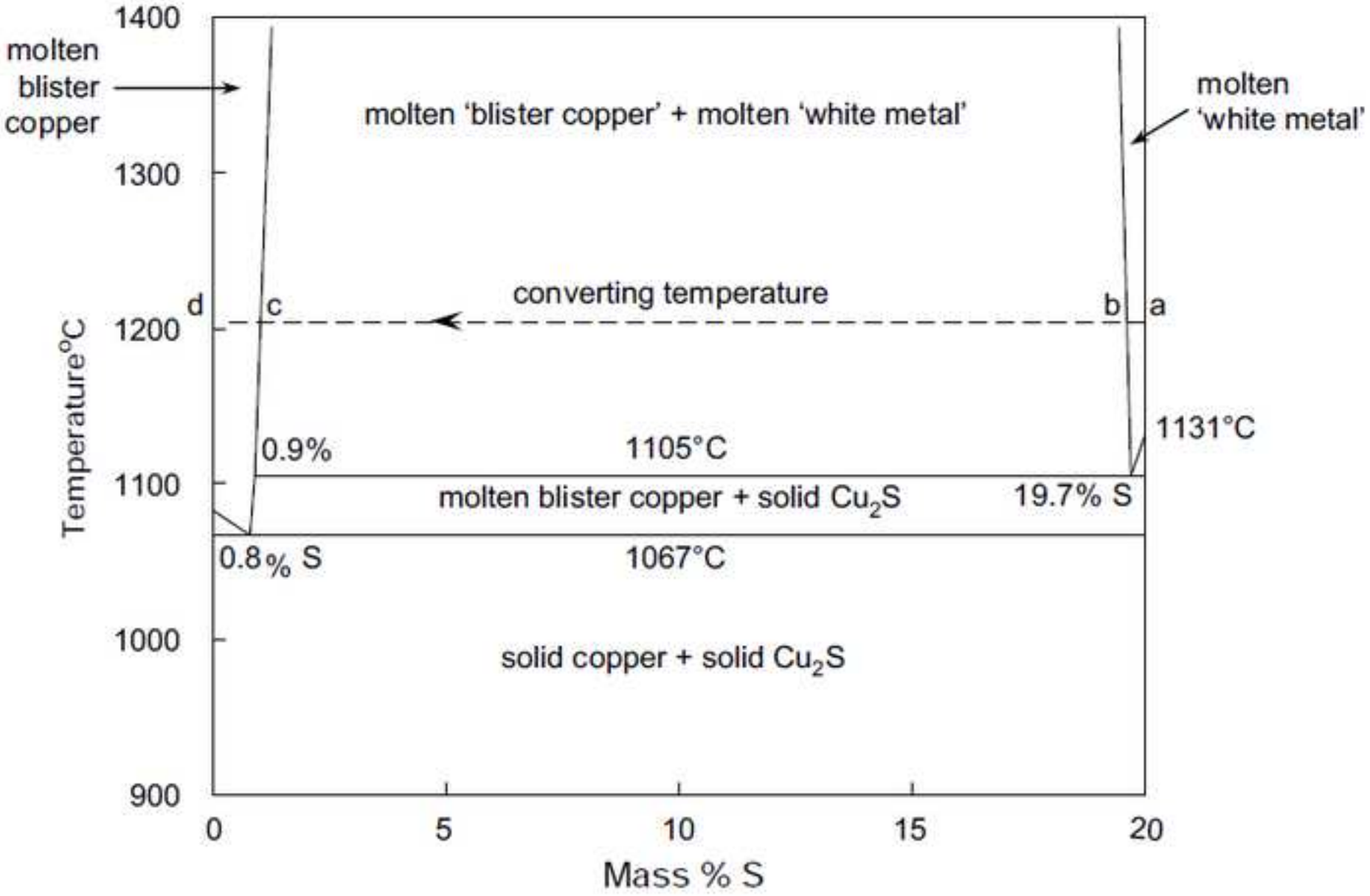

Figure 4

Click here to access/download;Figure;Fig 4 (DRX).png

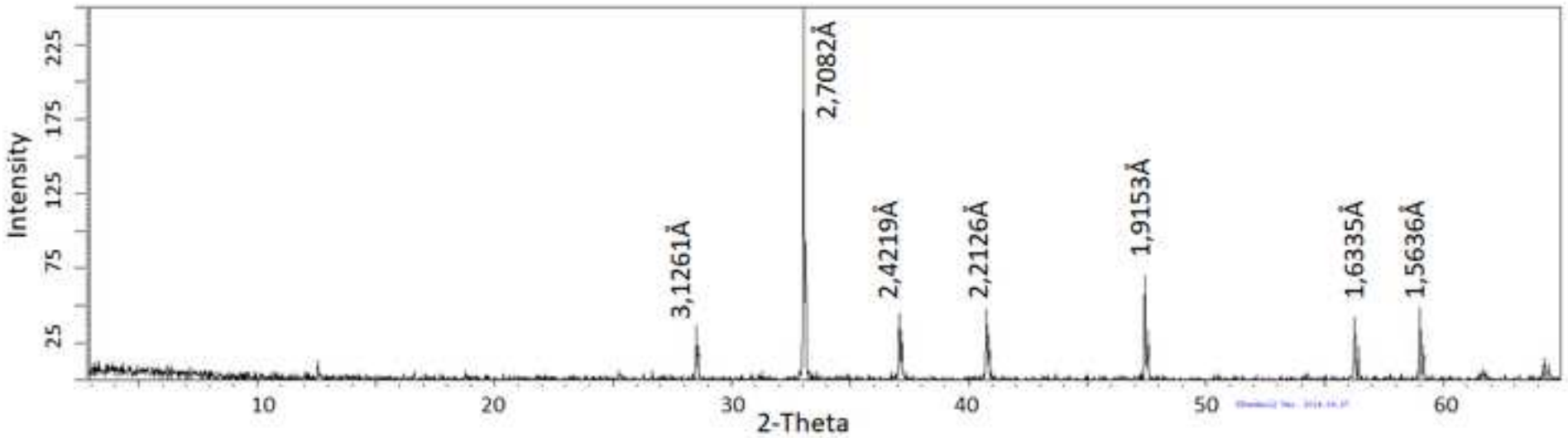

Figure 5

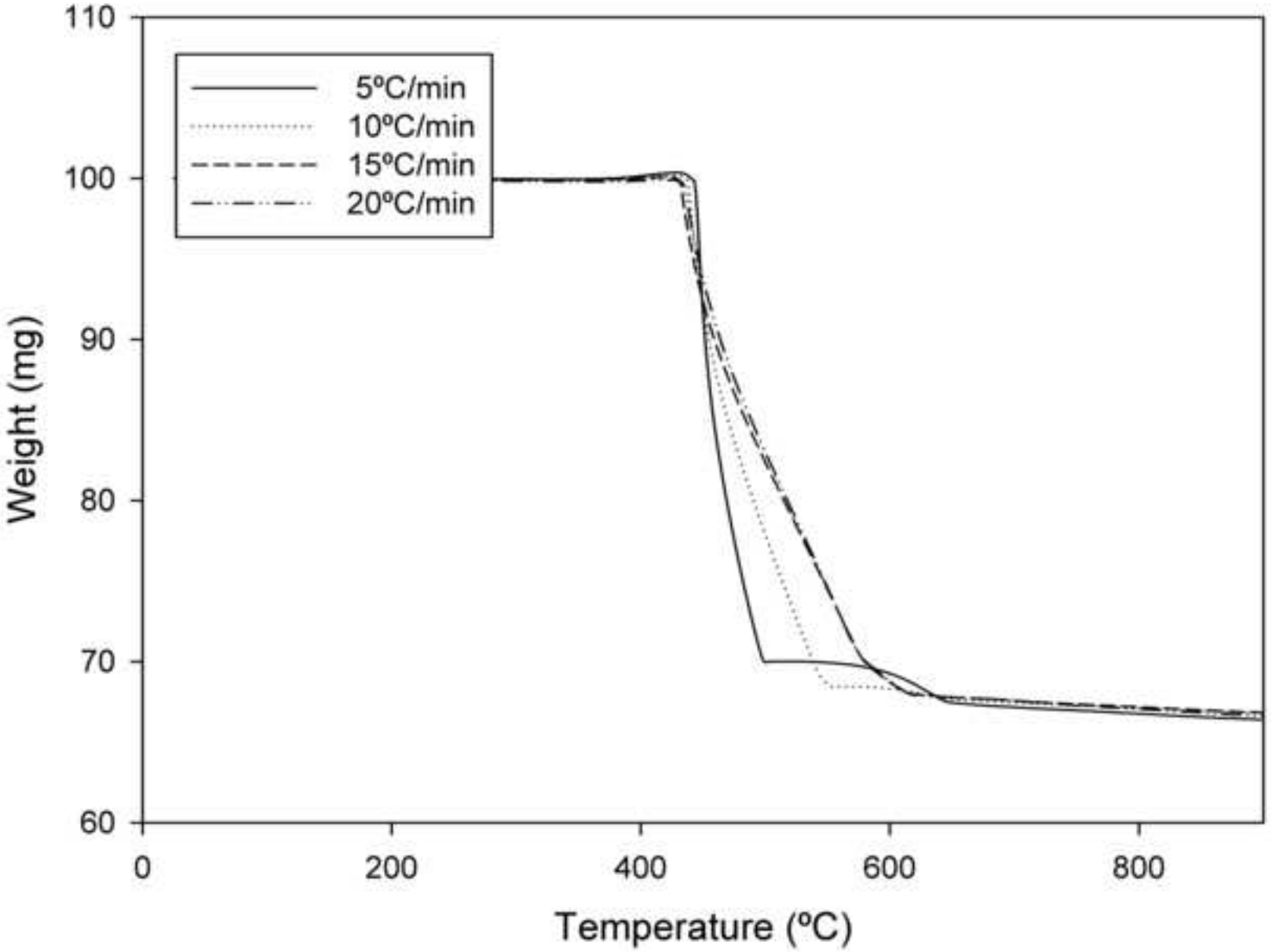

Figure 6

Click here to access/download;Figure;PIRITA FIG 6 DTG.JPG

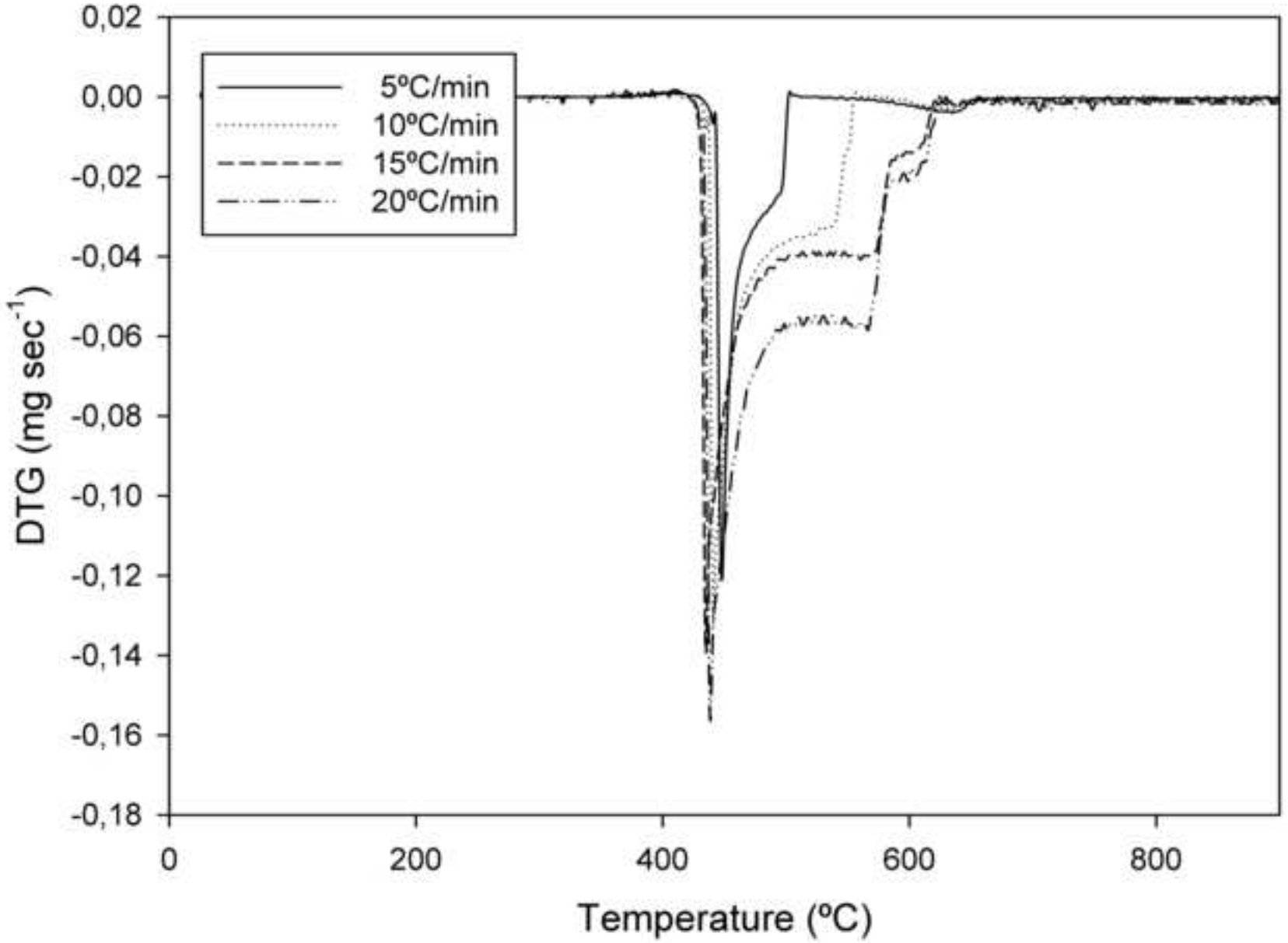

Figure 7

Click here to access/download;Figure;PIRITA FIG 7 KISSINGER ANALYSIS (bueno).JPG

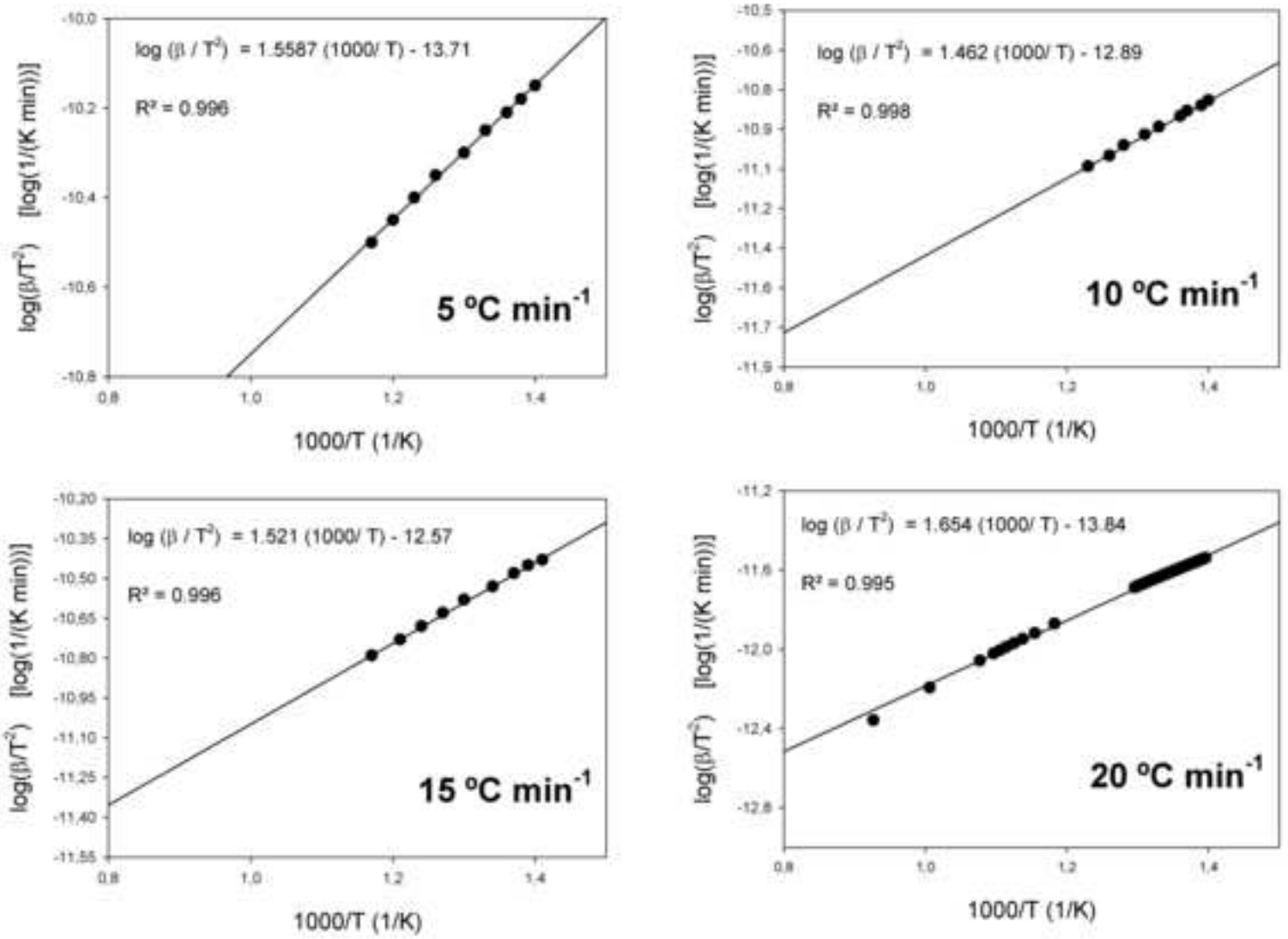

Figure 8

Click here to access/download;Figure;PIRITA FIG 8 EA (bueno).JPG

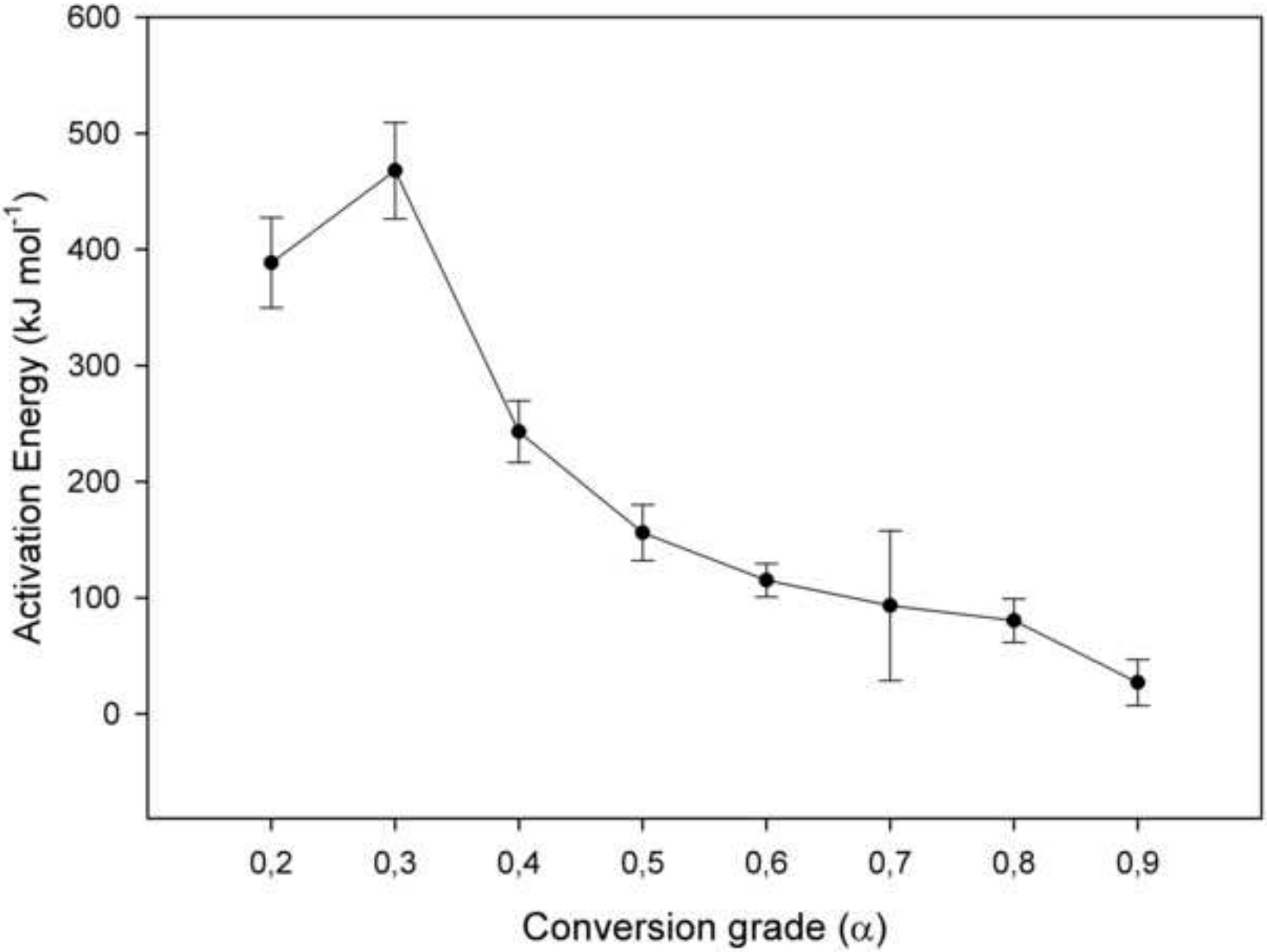

Figure 9

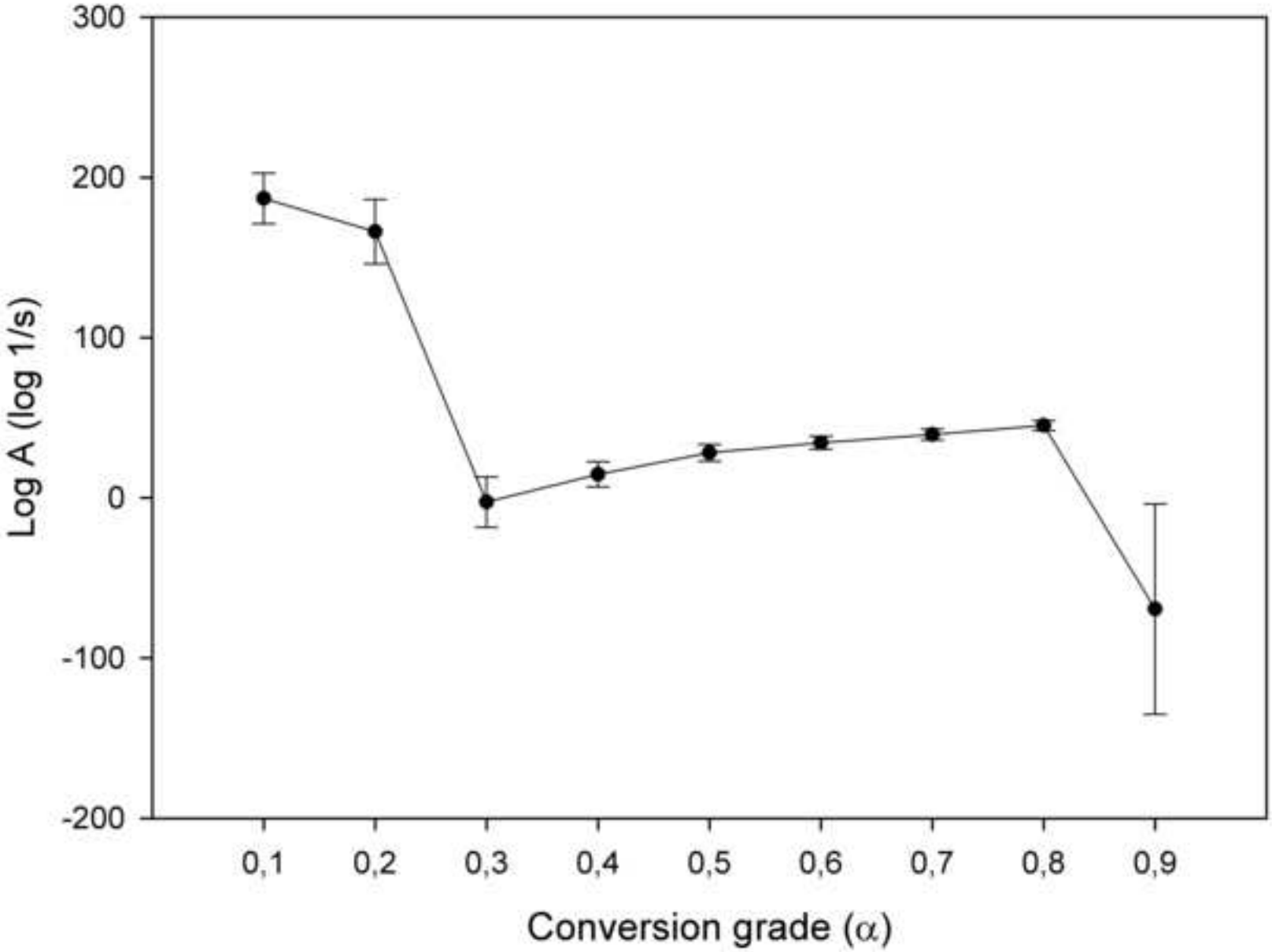

Table CAPT

Table 1. Statistical parameters for pyrite oxidative thermochemical behavior under several kinetic methods.

Table

1

Kinetic Method	R^2	Sum of dev. squares	Mean residuals	Student coef. 95%
ASTME1641–16	0.851	136415.21	9.45	1.9
Friedman	0.913	108294.27	7.26	1.9
Ozawa-Flynn-Wall	0.969	85452.26	6.07	1.9
KAS	0.992	564.13	1.09	1.9

2